Article:
Jiang, Jifu, Niu, Shuangxia and Zhao, Xing orcid.org/0000-0003-4000-0446 (2022) Quantitative Analysis of Hybrid-excited Doubly Salient Machine With Sub-slot Bottom PMs and Its Comparative Study. IEEE Transactions on Industrial Electronics. ISSN: 0278-0046

https://doi.org/10.1109/TIE.2022.3187571

Quantitative Analysis of Variable Reluctances Machine with Sub-slot Bottom PMs and its Comparative Study

Jifu Jiang, Shuangxia Niu, *Senior Member, IEEE* and Xing Zhao, *Member, IEEE*

***Abstract*—This paper propose a variable reluctance machine (VRM) with sub-slot bottom PMs to enhance the torque production. The key is that with auxiliary slot-PM excitation, the stator yoke DC saturation can be mitigated to enhance the torque production capability of DC field excitation, meanwhile additional slot-PM flux can be pushed into the airgap, which can build a parallel excitation and generate additional effective torque. Compared with slot-opening PM variable reluctance machine (SOPM-VRM), more AC slot space is saved for AC armature winding and higher AC armature current under the same current density can be fed into the sub-slot bottom PM variable reluctance machine (SBPM-VRM). In this case, torque and efficiency are improved by 43.5% and 12.0% under rated condition respectively. In this paper, torque separation effects due to DC field excitation and slot-bottom PMs are quantitatively analyzed with frozen permeability method. Then, SBPM-VRM, SOPM-VRM, and DC-excited VRM are compared under the same DC excitation. Also SBPM-VRM and COPM-VRM have the same PM usage. By using time-stepping finite-element analysis, the electromagnetic performances of three machines are evaluated. Experimental results verify validity of the proposed design.**

***Index Terms*—Sub-slot bottom PMs, slot opening PMs, torque separation, frozen permeability (FP).**

I. Introduction

VARIABLE reluctance machines (VRMs) can be categorized as no-independent excitation VRMs, DC-excited VRMs as well as PM excited VRMs in terms of different excitation sources [1-6]. DC-excitation VRMs have attracted more and more attention due to the increased price and limited supply of rare earth PM [7]. By regulating DC field current, DC-excited VRMs can realize flux adjustment easily, thus achieving variable speed constant output voltage and efficiency optimization for wind power generation [8-10]. However, it has relatively lower torque density and higher torque ripple compared with traditional PM machine [11]. In order to further enhance the torque density with less PM usage, some researchers begin to place the PMs in the slot opening. There are several kinds of slot-opening-PM machines. Radial magnetized PMs in the slot openings can enhance torque density through parallel excitation effect [12-13]. Tangential magnetized PMs in the slot openings can improve torque density through DC saturation relieving effect [14-20]. Moreover, a hybrid reluctance machine makes use of both radial and tangential PMs in the stator slot openings to advance the torque density with parallel excitation and DC saturation relieving effect respectively [21]. However, slot-opening PMs occupy AC slot space and leave less area placing AC armature winding, resulting in lower no-load back EMF and steady torque under the same AC current density.

This paper aims to presents two slot-PM assisted VRMs in which DC field excitation is combined with slot PMs to realize relatively high torque density and flux regulation capability. Comparing VRM placing PMs in the slot opening, the proposed VRM which has tangential magnetized PMs in the sub-slot bottom can increase AC slot space for placing AC armature winding with higher AC armature current under the same current density.

In the proposed machine, with a special slot-pole combination, non-salient effect is produced. Therefore, the total torque is the sum of the torque produced by DC field excitation and sub-slot bottom PMs. However, the stator core magnetization curve is non-linear, which will lead to inaccurate DC field and slot-bottom-PM field separation. Thus, torque separation accounting for the magnetic saturation and cross coupling is important for machine performance analysis. In previous research, frozen permeability (FP) has been applied to separate PM torque and reluctance torque in interior permanent magnet (IPM) machine [22]. In this paper, FP method is extended to separate torque produced by DC field excitation and sub-slot bottom PMs. In addition, open-circuit flux of two excitations is separated with FP method.

This paper is organized as following. In Section II, the machine structure and operation principle are introduced. In addition, flux is qualitatively and quantitatively analyzed. In section III, the leading design parameters are optimized to achieve maximum torque density and minimum torque ripple. In Section IV, open-circuit flux and on-load torque of DC field excitation and sub-slot bottom PMs are separated with FP method by the finite-element analysis (FEA). In Section V, the electromagnetic performance comparison among the proposed machine, slot opening PM design and DC-excited design under the same DC excitation is tested by FEA. Also, SBPM-VRM and SOPM-VRM have the same PM usage. Finally, a prototype is manufactured and test, some results and conclusions are drawn in Section VI and VII.

II. Machine Structure and Operation Principle

A. Machine Structures

Fig. 1 shows the topology of VRM with PMs placing in sub-slot bottom. The machine have a 24-slot stator and a 28-pole rotor. The robust rotor consists of only iron core with salient pole structure. The stator comprises all excitation sources, such as slot PMs, DC field excitation, and AC armature excitation. In addition, the machine adopts single-layer concentrated DC field winding and doubly-layer concentrated AC armature winding as shown in Fig. 1(b).

The merits of the proposed SBPM-VRM are listed as following.

1) The rotor possesses mechanical robustness and reliability with only iron core structure.
2) Flux bidirectional regulation capability can be achieved with flexibly adjusted DC excitation currents, thus more wind energy can be captured to extended speed range.
3) Tangential magnetized PMs in the sub-slot bottom can greatly enhancing the torque density with the parallel excitation and DC-saturation relieving effect when stator yoke is over saturated while stator teeth are unsaturated.
4) Since the armature magnetic flux does not pass through the sub-slot bottom PMs, there is no risk of demagnetization of sub-slot bottom PMs.
5) Comparing with slot-opening PMs, sub-slot bottom PMs do not occupy the area of AC slot and leave more space for AC armature winding, thus further improving the torque density with higher AC armature current injecting.

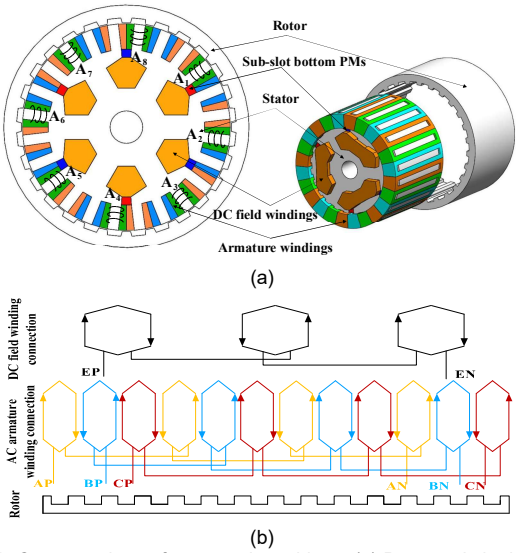

Fig. 1. Cross sections of proposed machines. (a) Proposed slot-bottom PM design. (b) Winding connection.

B. Slot-pole Combination of Both Machines

Due to the conventional combination of stator pole number, rotor pole number, DC field excitation pole number, as well as phase number, traditional VRMs suffer from not only asymmetric flux and back-EMF, but also large torque ripple. Two criteria are presented to solve abovementioned problems.

Firstly, every phase coils should be distributed in all locations relative to each DC field excitation pole [8]. Hence, coil number under a DC field excitation pole should be different from phase number, which can be expressed as:

$$(m+j)N_{dc} = N_s \tag{1}$$

where m is the phase number, while j is a positive integer and $j < m$. N_{dc} and N_s present DC field excitation pole and stator pole number.

Secondly, in order to preventing single-sided magnetic force, the difference between the number of rotor pole and stator pole is a multiple of two. The second criterion can be denoted as:

$$N_r = N_s \pm 2j_1 \tag{2}$$

where, j_1 is a positive integer. When $m = 3$ and $N_{dc} = 6$ is given, let $j = 1$, then $N_s = 24$ is deduced from (1). To achieve $N_r > N_s$, for proposed machine, let $j_1 = 2$, then $N_s = 28$ is deduced from (2). In this case, $N_s/N_r = 20/28$.

C. Flux Path Analysis of the proposed SBPM-VRM

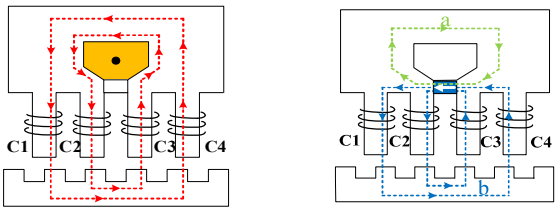

Fig. 2. Open-circuit flux distribution of 1/6 model in slot-bottom PM design. (a) Only DC excitation current. (b) Only sub-slot bottom PMs (Blue a: main flux linkage produces effective torque; green b: flux leakage relieves DC saturation).

Fig. 2 shows the open-circuit flux distribution under different excitation sources. Coil C1, C2, C3 and C4 are placed under four different angular positions relative to each DC excitation pole. When only DC excitation current is used as denoted in Fig. 2(a), the flux passes through stator yoke, stator teeth, airgap, and links the rotor and AC armature winding. It can be noticed that flux directions in C1 and C2 are negative, while flux direction in C3 and C4 are positive. When only sub-slot bottom PMs are applied as presented in Fig. 2(b), the flux has two magnetic circuits. One only links with stator and has opposite direction with the flux excited by DC excitation current as shown in green line *a* in Fig. 2(b). The other has the same magnetic circuit with DC excitation current, which passes through stator teeth, airgap, and links the rotor and AC armature winding as presented in blue line *b* in Fig. 2(b). It should be noticed that, if the stator yoke is far away from saturation, the whole flux excited by sub-slot bottom PMs will only links with the stator yoke. Along with stator yoke being more and more saturated with gradually increasing DC excitation current, more and more flux excited by sub-slot bottom PMs would pass through the stator teeth, airgap, and links the rotor and AC armature winding to generate effective back-EMF and steady torque. Meanwhile, some flux excited by sub-slot bottom PMs is still only associated with stator yoke to enhance back-EMF and steady torque produced by DC field excitation through DC saturation relieving effect. In this way, parallel excitation and DC saturation relieving of sub-slot bottom PMs only take into impact only when the stator yoke is over saturated while stator teeth are unsaturated. The two effects of torque production and DC saturation relieving are determined by the stator core

saturation condition. In other word, large DC excitation current lead to large DC excitation flux which pushes a plenty of sub-slot bottom PM flux entering into the airgap and rotor. It can be seen that flux directions in C1 and C2 are negative, while flux directions in C3 and C4 are positive.

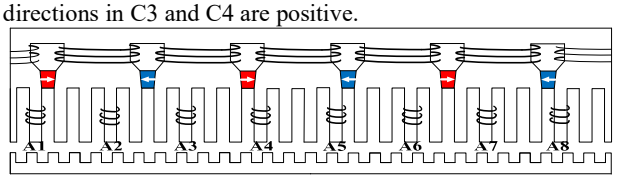

Fig. 3. Phase A coil distribution of .

As denoted in Fig. 3, Phase A is formed with eight coils, from coils A1 to A8. Among them, A1 to A4 are connected in series, which are classified as group I. A5 to A8 are connected in series, which are categorized as group II. Since group I and II are reversely connected, A1 and A5, A2 and A6, A3 and A7, A4 and A8 have the same flux waveform. Therefore, phase A flux linkage is twice the sum of flux linkage of coils A1, A2, A3 and A4. It can be noticed that coils A1, A2, A3 and A4 are placed at four different positions relative to each DC excitation pole. Comparing Fig .2 and Fig. 3, coil A1, A2, A3 and A4 are corresponding to C3, C1, C4 and C2 respectively. The only discrepancy between the corresponding coils lies in the phase difference. In terms of coils A1, A2, A3 and A4 distribution, the flux phase difference between then is equal to zero.

D. Frozen Permeability Principle and Procedure

The frozen permeability (FP) has been widely used to separate PM torque and reluctance torque in interior permanent magnet machine (IPMM), which is related with magnetic saturation and cross coupling issues. Since the proposed HEM machine has non-salient effect, FP method is proposed to separate torque produced by DC field excitation and slot-bottom PMs.

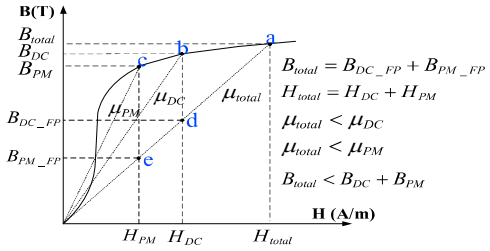

Fig. 4. FP concept diagram.

Fig. 4 shows the FP concept diagram. The subscripts "DC", "PM", "total" denotes DC field excitation, sub-slot bottom PMs, both DC field excitation and sub-slot bottom PMs. The total magneto-motive (magnetic field strength) H_{total} is the sum of H_{DC} and H_{PM}.

Under three different magnetic field strength H_{total}, H_{DC} and H_{PM}, the working points on the B-H curve are denoted as "a", "b", "c" respectively, then the resultant flux densities are marked as B_{total}, B_{DC} and B_{PM} respectively. It is obvious that $B_{DC} + B_{PM} < B_{total}$, which illustrating that the flux density of total field cannot be attained by simply superposition of flux density from DC field excitation and sub-slot bottom PMs.

With the FP method, the permeability will be fixed at a specific value μ_{total}, thus the nonlinear problem has been transformed into linear one. The DC field and slot-PM field can be decomposed. In other words, the B-H relationship transforms from a non-linear B-H curve to a straight line with a slope of μ_{total}. Hence, the working point under H_{DC} and H_{PM} are presented as "d" and "e", and corresponding flux densities are B_{DC_FP} and B_{PM_FP}. In this condition, the B_{total} is equal to the sum of B_{DC_FP} and B_{PM_FP}, which satisfies the linear superposition principle.

Fig. 5 gives the FP method procedure under open-circuit and on-load conditions. As shown in Fig. 6(a), under open-circuit condition, firstly, non-linear FE with all excitations (DC field excitation and sub-slot bottom PMs) is calculated. Then, permeability is frozen under this condition. Finally, DC excitation and slot-PM components with linear FE model are obtained based on above-calculated frozen permeability.

Comparing Fig. 5(a) with Fig. 5(b), the only difference between open-circuit and on-load condition lies in the addition of AC armature current in step 1 and step 3.

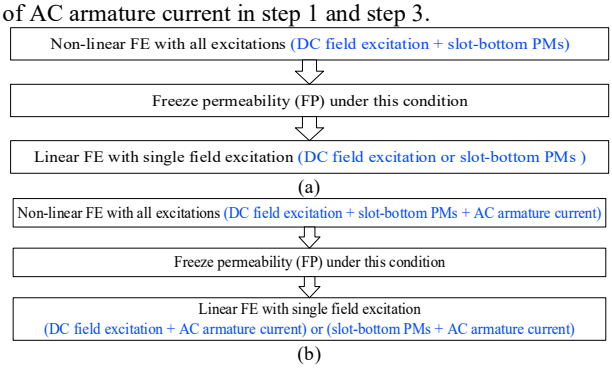

Fig. 5. FP method procedure. (a) Open-circuit condition. (b) On-load condition.

E. Flux Qualitative Analysis

To further explain the operation principle of slot-PM VRM with parallel-excited DC field excitation and sub-slot bottom PMs, the open-circuit flux in coil A1, A2, A3, A4 and phase A is analyzed using FP method.

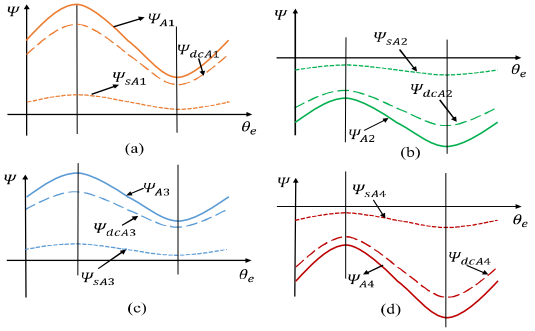

Fig. 6. Open-circuit flux linkage with different excitations. (a) Coil A1. (b) Coil A2. (c) Coil A3. (d) Coil A4.

With FP method as denoted in Fig. 6(a), while Ψ_{dcA1} and Ψ_{sA} represent the flux linkage in coil A1 excited by DC field excitation and sub-slot bottom PMs respectively, Ψ_{A1} denotes the total flux linkage in coil A1 with both excitations, as denoted in Fig. 6(a). Since coil A1 shares the same mechanical angle with DC field excitation and sub-slot bottom PM, Ψ_{dcA1} and Ψ_{sA1} have no phase shift. In addition, with FP frozen, the sum of Ψ_{dcA1} and Ψ_{sA1} is equal to Ψ_{A1}, which satisfies the linear superposition principle. Therefore, Ψ_{A1} can obtain the

maximum flux variation. In addition, A1 is corresponding to C3, thus Ψ_{dcA} and Ψ_{sA1} is positive. Hence, for coil A1, the flux linkage of sub-slot bottom PMs can greatly boost the positive biased flux linkage of DC field excitation.

Similarly, as presented in Fig. 6, for coil A2 to A4, Ψ_{A2} , Ψ_{A3} and Ψ_{A4} can attain the maximum flux variation, and flux linkage of sub-slot bottom PMs Ψ_{sA2} , Ψ_{sA3}, Ψ_{sA4} can greatly boost the biased flux linkage of DC field excitation Ψ_{dcA2}, Ψ_{dcA3} , Ψ_{dcA24}. Hence, in A1 to A4, flux with sub-slot bottom PMs can be an addition to flux with DC excitation current.

As shown in Fig. 7, due to the flux linkages excited by two excitations in coil A1, A2, A3 and A4 are entirely in phase, phase A flux linkage (Ψ_A) which is twice the sum of coil A1, A2, A3, A4 flux linkage (Ψ_{A1}, Ψ_{A2}, Ψ_{A3}, Ψ_{A4}) can achieve the maximum flux variation. Additionally, since coils A1 and A4, A2 and A3 are located in symmetrical positions with respect to a DC excitation pole, flux linkage DC component in coils A1 and A4 possess the same amplitude, but in different flux direction, thus counteracting each other thoroughly. Similarly, the flux linkage DC component in coils A2 and A3 also compensate each other definitely. Therefore, the phase A flux linkage has no biased DC component, thus stator core is less likely to be saturated.

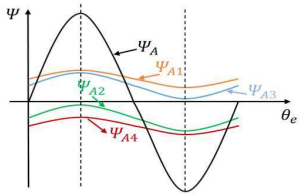

Fig. 7. Open-circuit flux linkage.

The slot-PM flux associating with the AC armature winding and the rotor can produce effective torque which can be superimposed with the torque produced by DC field excitation. Also, the slot-PM flux only related with stator can relieve stator core saturation and enhance the stator core utilization factor, thus improving torque excited by DC field current.

F. Flux Quantitative Analysis

The flux linkage excited by DC field excitation in four different coils A1, A2, A3 and A4 are denoted as Ψ_{dcA1}, Ψ_{dcA2}, Ψ_{dcA3} and Ψ_{dcA4}, which can be expressed as

$$\begin{cases} \psi_{\mathrm{dcA1}} = \psi_{dcDCA1} + \sum_{n=1}^{+\infty} \psi_{dcACA1n} \cos(nP_r\theta_r) \\ \psi_{\mathrm{dcA2}} = -\left\{ \psi_{dcDCA2} + \sum_{n=1}^{+\infty} \psi_{dcACA2n} \cos[nP_r(\theta_r - \frac{2\pi}{P_s}\times 3)] \right\} \\ \psi_{\mathrm{dcA3}} = \psi_{dcDCA3} + \sum_{n=1}^{+\infty} \psi_{dcACA3n} \cos[nP_r(\theta_r - \frac{2\pi}{P_s}\times 6)] \\ \psi_{\mathrm{dcA4}} = -\left\{ \psi_{dcDCA4} + \sum_{n=1}^{+\infty} \psi_{dcACA4n} \cos[nP_r(\theta_r - \frac{2\pi}{P_s}\times 9)] \right\} \end{cases} \quad (3)$$

where Ψ_{dcDCA1}, Ψ_{dcDCA} , Ψ_{dcDCA3} and Ψ_{dcDCA} are the DC component of flux linkage excited by DC field excitation in coils A1, A2, A3 and A4. Ψ_{dcACA} , $\Psi_{dcACA2n}$, $\Psi_{dcACA3n}$ and Ψ_{dcACA} are the magnitude of *n*th harmonics of flux linkage excited by DC field excitation in coils A1, A2, A3 and A4.

The flux linkage excited by sub-slot bottom PMs in four different coils A1, A2, A3 and A4 are denoted as Ψ_{sA1}, Ψ_{sA2}, Ψ_{sA3} and Ψ_{sA4}, which can be presented as

$$\begin{cases} \psi_{\mathrm{sA1}} = \psi_{sDCA1} + \sum_{n=1}^{+\infty} \psi_{sACA1n} \cos(nP_r\theta_r) \\ \psi_{\mathrm{sA2}} = -\left\{ \psi_{sDCA2} + \sum_{n=1}^{+\infty} \psi_{sACA2n} \cos[nP_r(\theta_r - \frac{2\pi}{P_s}\times 3)] \right\} \\ \psi_{\mathrm{sA3}} = \psi_{sDCA3} + \sum_{n=1}^{+\infty} \psi_{sACA3n} \cos[nP_r(\theta_r - \frac{2\pi}{P_s}\times 6)] \\ \psi_{\mathrm{sA4}} = -\left\{ \psi_{sDCA4} + \sum_{n=1}^{+\infty} \psi_{sACA4n} \cos[nP_r(\theta_r - \frac{2\pi}{P_s}\times 9)] \right\} \end{cases} \quad (4)$$

where Ψ_{sDCA1} , Ψ_{sDCA2} , Ψ_{sDC} and Ψ_{sDCA4} are the DC component of flux linkage excited by slot-bottom PMs in coils A1, A2, A3 and A4. Ψ_{sACA1} , Ψ_{sACA2n}, Ψ_{sACA3n} and Ψ_{sACA4} are the magnitude of *n*th harmonics of flux linkage excited by slot-bottom PMs in coils A1, A2, A3 and A4.

After using the FP method, the flux excited by two excitations can satisfy the linear superposition principle. In addition, due to coils A1 and A4, A2 and A3 are located in symmetrical positions with respect to a DC excitation pole, $\Psi_{dcDCA1} = \Psi_{dcDCA4}$, $\Psi_{dcD} = \Psi_{dcDCA3}$, $\Psi_{dcA} = \Psi_{dcACA4n}$ $\Psi_{dcACA} = \Psi_{dcA}$, $\Psi_{sDCA1} = \Psi_{sDCA4}$, $\Psi_{sDCA2} = \Psi_{sDCA}$, $\Psi_{sACA1n} = \Psi_{sACA4}$ $\Psi_{sACA2} = \Psi_{sACA3}$. Hence, the flux excited by both DC field excitation and sub-slot bottom PMs in coils A1, A2, A3, and A4 can be denoted as

$$\begin{cases} \psi_{\mathrm{A1}} = \psi_{\mathrm{yA1}} + \psi_{\mathrm{sA1}} \\ \quad = (\psi_{dcDCA1} + \psi_{sDCA1}) + \sum_{n=1}^{+\infty} (\psi_{dcACA1n} + \psi_{sACA1n}) \cos(nP_r\theta_r) \\ \psi_{\mathrm{A2}} = \psi_{\mathrm{yA2}} + \psi_{\mathrm{sA2}} \\ \quad = -(\psi_{dcDCA2} + \psi_{sDCA2}) \\ \quad\quad - \sum_{n=1}^{+\infty} (\psi_{dcACA2n} + \psi_{sACA2n}) \cos[nP_r(\theta_r - \frac{2\pi}{P_s}\times 3)] \\ \psi_{\mathrm{A3}} = \psi_{\mathrm{yA3}} + \psi_{\mathrm{sA3}} \\ \quad = (\psi_{dcDCA3} + \psi_{sDCA3}) \\ \quad\quad + \sum_{n=1}^{+\infty} (\psi_{dcACA3n} + \psi_{sACA3n}) \cos[nP_r(\theta_r - \frac{2\pi}{P_s}\times 6)] \\ \psi_{\mathrm{A4}} = \psi_{\mathrm{yA4}} + \psi_{\mathrm{sA4}} \\ \quad = -(\psi_{dcDCA4} + \psi_{sDCA4}) \\ \quad\quad - \sum_{n=1}^{+\infty} (\psi_{dcACA4n} + \psi_{sACA4n}) \cos[nP_r(\theta_r - \frac{2\pi}{P_s}\times 9)] \end{cases} \quad (5)$$

According to (5), flux linkage excited by DC field excitation and sub-slot bottom PMs is superposed in coils A1 to A4. Since phase A flux linkage is twice the sum of coils A1, A2, A3 and A4 flux linkage. Therefore, flux of phase A can be expressed as

$$\begin{aligned} \psi_A &= 2\times(\psi_{\mathrm{A1}} + \psi_{\mathrm{A2}} + \psi_{\mathrm{A3}} + \psi_{\mathrm{A4}}) \\ &= -4\times \sum_{n=1,3,5\ldots}^{+\infty} (\psi_{yACA1n} + \psi_{sACA1n}) \sin(9n\pi\frac{P_r}{P_s}) \sin[nP_r(\theta_r - \frac{9\pi}{P_s})] \\ &\quad + 4\times \sum_{n=1,3,5\ldots}^{+\infty} (\psi_{yACA2n} + \psi_{sACA2n}) \sin(3n\pi\frac{P_r}{P_s}) \sin[nP_r(\theta_r - \frac{9\pi}{P_s})] \end{aligned} \quad (6)$$

It can be concluded from (6) that DC component and even odd harmonics of phase A flux linkage can be eliminated with special slot-pole combination. Since high order harmonics can be ignored, only fundamental harmonics of phase flux linkage remains, thus phase flux linkage is pretty sinusoidal. In addition, flux variation is superimposed with two excitations.

III. Design Optimization

A. Design Optimization

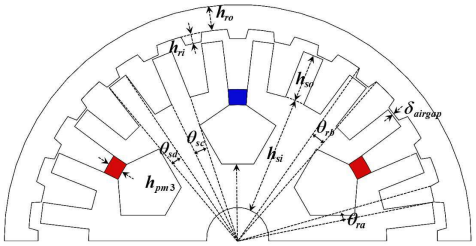

Fig. 8. Dimension parameters of the proposed SBPM-VRM.

TABLE I
FUNDAMENTAL DATA OF SBPM-VRM

Rated voltage	V	60
Rated torque	T	12
Rated speed	rpm	600
Number of turns per AC armature coil	/	40
Number of turns per DC field coil	/	400
PM remanence	T	1.1
PM coercivity	kA/m	838
Steel saturated flux density	T	1.8
Steel mass density	kg/m	7820

TABLE II
INITIAL DIMENSION PARAMETERS OF SBPM-VRM

Symbol	Parameter	Unit	Value
R_{ro}	Outer radius of rotor	mm	75
R_{si}	Inner radius of stator	mm	67
h_{ro}	Height of rotor yoke	mm	8
h_{ri}	Height of rotor slot	mm	5
h_{so}	Height of stator slot	mm	16
h_{si}	Height of stator yoke	mm	37.4
l	Stack length	mm	80
δ_{airgap}	Airgap length	mm	0.6
h_{pm}	Height of slot-PMs	mm	5
θ_{ra}	Arc of rotor tooth top	rad	0.1086
θ_{rb}	Arc of rotor tooth bottom	rad	0.1310
θ_{sc}	Arc of stator tooth bottom	rad	0.1116
θ_{sd}	Arc of stator tooth top	rad	0.0854

Later, FEA models with 24/28 slot-pole combination is analysed. Fundamental data of proposed machine is given in Table I, Dimension parameters are depicted in Fig. 8 and initial values of dimension parameters are shown in Table II.

In this paper, the maximum torque density and minimum torque ripple are taken as two optimization objectives. The optimization result of last generation is denoted in Fig. 10. Before the turning point, along with the enhancement of average torque, torque ripple increases slowly. However, torque ripple increases exponentially after the turning point. In this case, the stator core is saturated, main flux cannot increase and torque cannot improve, while flux leakage increases which leads to large torque ripple. A multi-objective optimization can cause plenty of unsuitable cases. A few of relative optimal elements are found at the turning points, which possess relatively high average torque and lower torque ripple, as shown in red circle in Fig. 9. Table III shows the dimension parameters and their optimal values

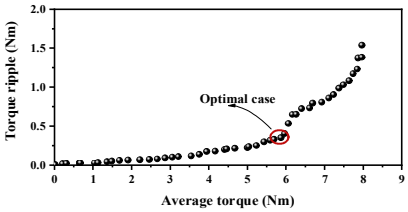

Fig. 9. Optimization results of the last generation.

TABLE III
DIMENSIONS OF THE PROPOSED SBPM-VRM

Parameter	Lower Limit	Upper Limit	Initial value	Optimal value
h_{ro} (mm)	4	16	8	7.83
h_{ri} (mm)	2	12	5	2.99
θ_{ra} (rad)	0.08	0.16	0.1086	0.08
θ_{rb} (rad)	0.10	0.18	0.1310	0.1024
h_{so} (mm)	9	30	16	15.70
h_{si} (mm)	35	65	37.4	41.88
θ_{sc} (rad)	0.10	0.20	0.1116	0.1326
θ_{sd} (rad)	0.08	0.18	0.0854	0.1064
h_{pm3} (mm)	1	10	4	5

IV. Electromagnetic Performance Analysis

Using the commercial software Ansys Maxwell and FP method, finite-element simulation is carried out to assess the electromagnetic performance of the proposed machine.

A. Flux Separation with FP Method under Open-circuit condition

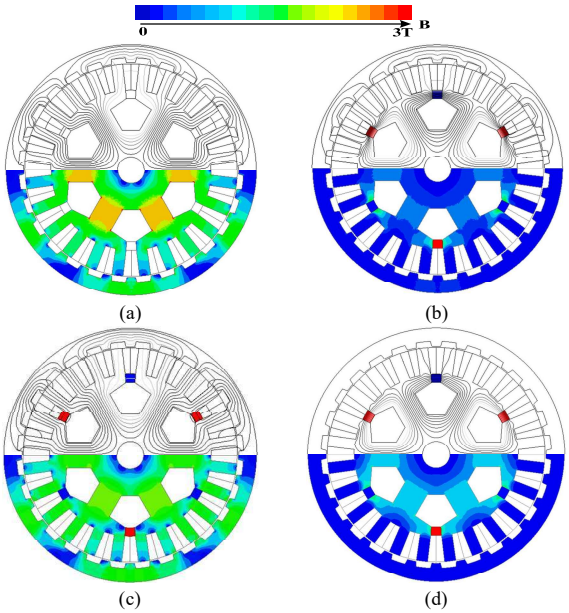

Fig. 10. Open-circuit flux distribution with FP method. (a) Only DC field excitation. (b) Only sub-slot bottom PMs. (c) Both excitations. (d) Only sub-slot bottom PMs with lower DC field current.

Fig. 10 shows the open-circuit flux distribution under different excitation status with FP method as shown in Fig. 5(a). It is denoted that both DC field excitation and sub-slot bottom PMs have the same pole pair number and share a parallel magnetic circuit. As for only 12 A/mm^2 DC field excitation, the flux passes through the stator, airgap, links the rotor, and then goes back to stator, which is denoted in Fig. 10(a). As for only sub-slot bottom PMs, the majority of flux passes through the stator yoke, which direction is opposite to that produced by the DC field excitation, thus relieving DC saturation of the stator core. Some flux goes through the airgap, links the rotor and armature winding to produce effective torque, which is shown in Fig. 10(b). Comparing flux density distribution in Fig. 10(a) and Fig. 10(c), the stator yoke is less saturated with introducing of sub-slot bottom PMs. Fig. 10(d) gives only sub-slot bottom-PM flux distribution under FP of both 6 A/mm^2 DC field excitation and sub-slot bottom PMs. Comparing Fig. 10(b) and Fig. 10(d), the higher the DC field excitation, the more slot-bottom-PM flux will be pushed into airgap, link rotor and armature winding to produce torque.

Using FP method, the open-circuit flux linkage waveforms and corresponding harmonics in coils A1, A2, A2 and A4 are presented in Fig. 11. It can be seen that, for coil A1 to A4, slot-PM flux linkage can boost the biased DC field excitation flux linkage. The total coil flux is equal to the flux excited by only DC field excitation and only sub-slot bottom PMs.

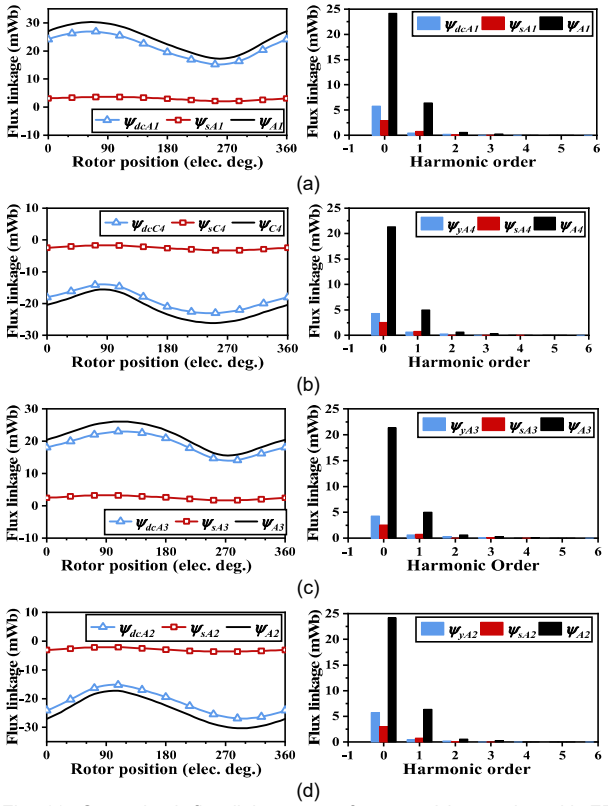

Fig. 11. Open-circuit flux linkage waveforms and harmonics with FP method. (a) Coil A1. (b) Coil A2. (c) Coil A3. (4) Coil A4.

The open-circuit flux linkage waveforms of phase A and the corresponding harmonics are shown in Fig. 12. It can be found in Fig. 12(a) that flux linkages of coils A1, A2, A3 and A4 have no phase shift, phase A flux linkage can obtain the maximum flux linkage variation. Also, the flux linkages of coils A1 and A3 are positive while coils A2 and A4 are negative. The harmonics of flux linage in coils A1 and A4 are in the same amplitude. The same in coils A2 and A3, which can be seen in Fig. 12(b). Then, the even order harmonics of flux linkage in phase A are eliminated which is in accordance with Eq. (6) in section II. Since high order harmonics are pretty small and can be ignored, the phase A flux linkage is perfect sinusoidal.

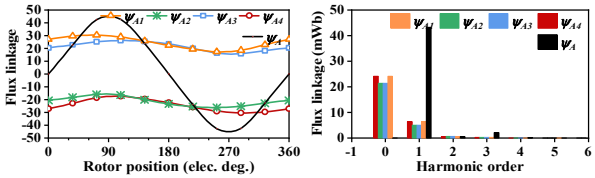

Fig. 12. Open-circuit flux linkage with FP method. (a) Waveforms. (b) Harmonics.

B. *Torque Separation with FP Method Under On-load condition*

Fig. 13 shows steady torque under rated condition with 12 A/mm^2 DC field and 6 A/mm^2 AC armature current density using FP method. It can be noticed that torque with only DC field excitation and only sub-slot bottom PMs are 11.4 Nm and 1.6 Nm. Also, torque with both excitations is 13.0 Nm, which is the sum of torque with only DC field excitation and only sub-slot bottom PMs. The torque excited by sub-slot bottom PMs account for 12% of the torque excited by both excitations.

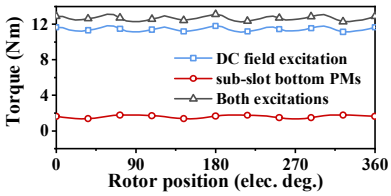

Fig. 13. Steady torque under rated condition with FP method.

Fig.14(a). shows torque varied with the increase of AC armature current density under 12 A/mm^2 DC field current using FP method. It can be found that torque with only DC field excitation and both excitations are improved with the increase of AC armature current density. Meanwhile, the torque with sub-slot bottom PMs is enhanced first, and then attains a constant value. Moreover, the torque with both excitations is the sum of that with only DC field excitation and only sub-slot bottom PMs. Fig. 14(b) gives torque varied with the increase of DC field current density under 6 A/mm^2 AC armature current using FP method. It can be found that torque with DC field excitation and both excitations are enhanced along with the increase of DC field current density and almost coincides with each other when the DC field current density is lower than 6 A/mm^2. When the DC field current density is higher than 6 A/mm^2, two curves attain a platform, and even lower down a little, which is due to the stator core saturation. The torque with sub-slot bottom PMs maintain zero between 0 to 6 A/mm^2, since the stator core is not saturated and sub-slot bottom PMs has no function. The torque with sub-slot bottom PMs increases between 6 A/mm^2 to 12 A/mm^2 DC field current density along with the stator core is more and more saturated, and remains constant when DC field current density is higher than 12 A/mm^2

when the stator core is over saturated. It can be concluded that the higher DC current density between 6 A/mm^2 to 12 A/mm^2, the higher the torque excited by sub-slot bottom PMs.

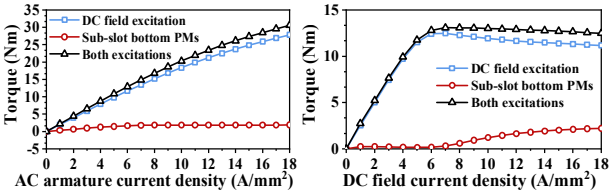

Fig. 14. Torque varied with current density with FP method. (a) AC armature current. (b) DC field current.

V. Machine Comparative Study

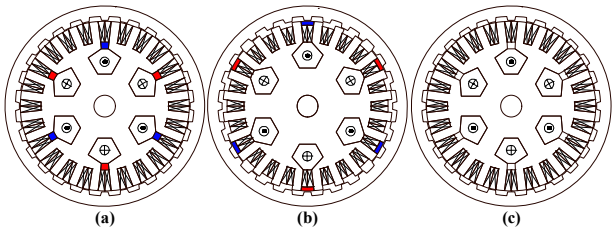

Fig. 15. Cross sections of three machines. (a) SBPM-VRM. (b) SOPM-VRM. (c) DC-excited VRM.

In order to validate the advantage of sub-slot bottom PMs over slot-opening PMs, three machines without slot PMs, with PMs placed in the slot opening and sub-slot bottom, namely DC-excited VRM, SOPM-VRM, and SBPM-VRM, are compared in detail as shown in Fig. 15. To achieve a fair comparison, the stator diameter, stack length, slot-pole combination, ac/dc current density, and ac/dc slot space are kept the same. In addition, SOPM-VRM and SBPM-VRM have the same PM usage.

Fig. 16 gives the no-load flux linkage and back-EMF of three machines under rated condition of 6 A/mm^2 AC current density and 12 A/mm^2 DC current density. It can be seen that the SBPM-VRM has the highest amplitude of flux linkage and back-EMF among three machines.

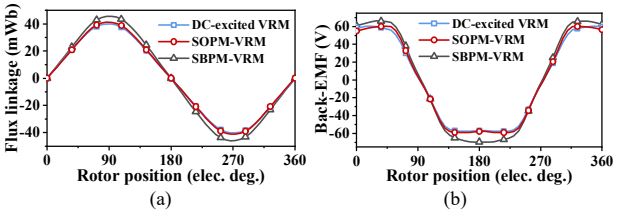

Fig. 16. No-load electromagnetic performances of three machines. (a) Flux linkage. (b) Back-EMF

Fig. 17 presents flux linkage against different DC field current density in AC armature winding and stator yoke. As shown in Fig. 17(a), AC flux linkages of three machines increase rapidly when DC field current density is lower than 7 A/mm^2, and which attains a platform when DC field current density is higher than 7 A/mm^2. Comparing SBPM-VRM and DC-excited VRM, difference between them is highest in 7 A/mm^2 with DC saturation relieving effect of sub-slot bottom PMs, and reduces with the increase of DC current density since the stator core is over-saturated. As for SOPM-VRM, the flux linkage slightly decreases when the DC current density is higher than 7 A/mm^2 since stator teeth is over-saturated. Fig. 17(b) shows flux in stator yoke against different DC field current density. Yoke flux of DC-excited VRM is the highest when DC current density is lower than 7 A/mm^2, which illustrates the stator core saturation relieving effect of both the slot-opening PMs and sub-slot bottom PMs.

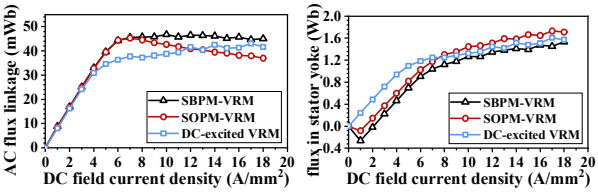

Fig. 17. Flux linkage against different DC field current density. (a) AC winding. (b) Stator yoke.

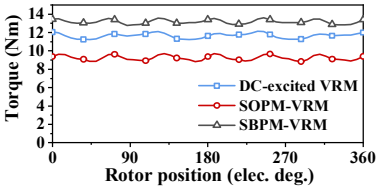

Fig. 18. Steady torque waveform of three machines.

Fig. 18 denotes steady torque of three machines. It can be calculated that torque with DC-excited VRM, SOPM-VRM and SBPM-VRM are 11.7 Nm, 9.2 Nm and 13.2 Nm. Comparing DC-excited VRM and SBPM-VRM, the steady torque can be enhanced by 12.8% with the use of sub-slot bottom PMs. Comparing SOPM-VRM and SBPM-VRM, the steady torque can be improved by 43.5% through moving PMs from slot opening to sub-slot bottom, since more AC space can be left for placing AC armature winding with higher armature current under the same current density. SOPM-VRM has lowest torque with lowest AC armature current with smallest AC slot space.

I. Experimental Validation

A SBPM-VRM prototype is manufactured, and dimension parameters are given in Table I, II and III. The prototype is tested to verified electromagnetic performances of proposed machine. Fig. 19 gives stator core, winding connection and robust rotor. Fig. 20 presents a test platform, which includes prototype, DC power supply, dSPACE, dynamometer, oscilloscope, inverter, as well as control panel.

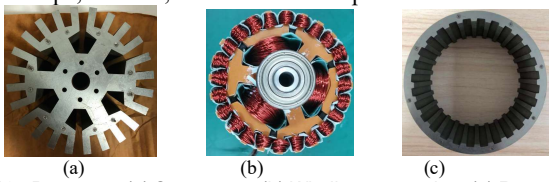

Fig. 19. Prototype. (a) Stator core. (b) Winding connection. (c) Rotor.

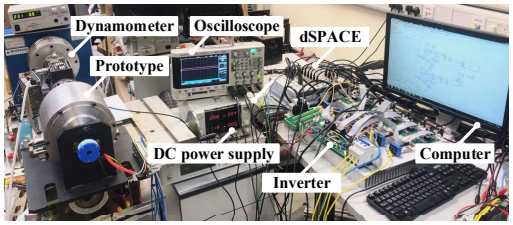

Fig. 20. Test platform.

When the machine operates at 600 rpm, with the use of oscilloscope, the measured open-circuit back-EMF waveform

of phase A is shown in Fig. 21. It can be noticed that the back-EMF realizes three phase symmetric and the amplitude of back-EMF is 69V. Test result is consistent with FEA results.

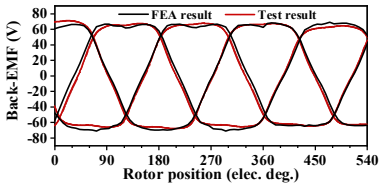

Fig. 21. Measured open-circuit back-EMF at 600 rpm.

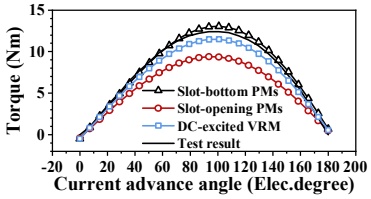

Fig. 22. Measured torque against current advance angle.

Fig. 22 shows torque against current advance angle, and SBPM-VRM has the highest torque among three machines in all current advance angle. The curves of three machines are all sinusoidal, indicating the non-salient effect with pretty small torque ripple. In addition, the measured result of SBPM-VRM coincides with the simulation result.

Fig. 23 presents torque against different AC/DC current density. It can be found that the torque of SBPM-VRM is highest among three machines in all AC current density. The difference of them becomes slightly bigger with the increase of AC current density along with the enhancing DC saturation relieving and parallel excitation effect of sub-slot bottom PMs. In addition, the measure result of SBPM-VRM agrees well with the simulation result.

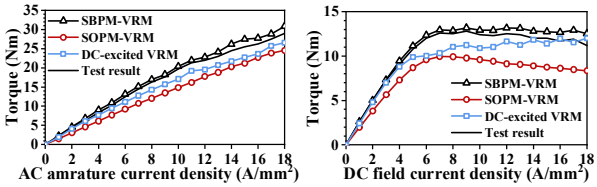

Fig. 23. Measured torque against current density. (a) AC armature current. (b) DC field current.

As shown in Fig. 24, the efficiency of SBPM-VRM is highest among three machines. Furthermore, the measured efficiency of SBPM-VRM coincided with simulation result.

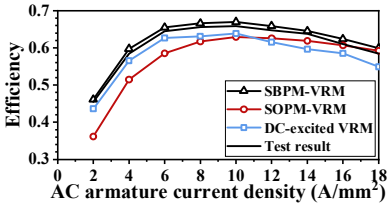

Fig. 24. Measured efficiency against current density.

II. Conclusion

This paper proposes a novel VRM with sub-slot bottom PMs, which enhances effective torque with parallel excitation and DC-saturation relieving effects, thus stator core utilization factor can be improved. Through flux analysis, with special slot-pole combination, DC component and even order harmonics of phase flux are eliminated, thus smooth torque can be attained. Then, the proposed SBPM-VRM is optimized with maximum average torque and minimum torque ripple. Additionally, open-circuit flux separation and on-load torque separation of the optimized machine with FP method are analyzed. The torque with sub-slot bottom PMs 1.6 Nm accounts for 12% of the torque with two excitations 13 Nm. It verified that the torque with both excitations is the sum of the torque with DC field excitation and slot-bottom PMs respectively using FP method.

Comparing with SBPM-VRM, SOPN-VRM and DC-excited VRM, the torque of SBOM-VRM is 13.2 Nm, which is enhanced by 12.8% comparing with DC-excited VRM and improved by 43.5% comparing with SOPM-VRM. With the increase of AC/DC current density, the DC-saturation-relieving and parallel excitation effect of the slot-bottom PMs become more and more obvious. In addition, moving PM from slot opening to sub-slot bottom, there are more AC slot space placing armature winding, resulting in larger armature current under the same current density. Finally, a prototype is manufactured to validate the theoretical analysis. The experimental results agree well with the simulation results, which also consists with the theoretical analysis. It is concluded that SBPM-VRM has highest torque, efficiency along with different AC/DC current density.

References

[1] D. Lee, T. H. Pham, "Design and Operation Characteristics of Four-Two Pole High-Speed SRM for Torque Ripple Reduction," *IEEE Trans. Ind. Elec.*, vol. 60, no. 9, pp. 3637-3643, Sept. 2013.

[2] W. Ding, "Performance Improvement for Segmented-Stator Hybrid-Excitation SRM Drives Using an Improved Asymmetric Half-Bridge Converter," *IEEE Trans. Ind. Elec.*, vol. 66, no. 2, pp. 898-909, Feb. 2019.

[3] Y. Fan, K. T. Chau, and M. Cheng, "A new three-phase doubly salient permanent magnet machine for wind power generation," *IEEE Trans. Ind. Appl.*, vol. 42, pp. 53–60, 2006.

[4] M. M. Radulescu, "A new electronically-commutated doubly-salient permanent-magnet small motor," 1995 Seventh International Conference on Electrical Machines and Drives, 1995, pp. 213-216.

[5] G. Ming, L. Wu, "Comparative Study of Novel Doubly Fed Doubly Salient PM Machines with Different Stator/Rotor-Pole Number Combinations," *IEEE Trans. Magn.*, vol. 57, no. 6, pp. 1-5, June 2021.

[6] K. T. Chau, J. Z. Jiang and Yong Wang, "A novel stator doubly fed doubly salient permanent magnet brushless machine," *IEEE Trans. Magn.*, vol. 39, no. 5, pp. 3001-3003, Sept. 2003.

[7] A. Kohara, K. Hirata and N. Niguchi, "Vibration Comparison of Current Superimposition Variable Flux Machine and Switched Reluctance Machine," 2018 XIII International Conference on Electrical Machines (ICEM), 2018, pp. 2337-2342.

[8] J. Bao, B. L. J. Gysen, K. Boynov, "Torque Ripple Reduction for 12-Stator/10-Rotor-Pole Variable Flux Reluctance Machines by Rotor Skewing or Rotor Teeth Non-Uniformity," *IEEE Trans. Magn.*, vol. 53, no. 11, pp. 1-5, Nov. 2017.

[9] X. Liu and Z. Q. Zhu, "Comparative Study of Novel Variable Flux Reluctance Machines with Doubly Fed Doubly Salient Machines," *IEEE Trans. Magn.*, vol. 49, no. 7, pp. 3838-3841, July 2013.

[10] Y. Fan, K. T. Chau and S. Niu, "Development of a New Brushless Doubly Fed Doubly Salient Machine for Wind Power Generation," *IEEE Trans. Magn.*, vol. 42, no. 10, pp. 3455-3457, Oct. 2006.

[11] K. T. Chau, M. Cheng, "Nonlinear magnetic circuit analysis for a novel stator doubly fed doubly salient machine," *IEEE Trans. Magn.*, vol. 38, pp. 2382–2384, 2002

[12] X. zhao, S. Niu, W Fu, "A novel vernier reluctance machine excited by slot PMs and zero-sequence current for electric vehicle," *IEEE Trans. Magn.*, vol. 55, no. 6, pp. 1-5, Jun. 2019.

[13] X. zhao, S. Niu, "Design and optimization of a novel slot-PM-assisted variable flux reluctance generator for hybrid Electric vehicles," *IEEE Trans. Energy Convers.*, vol. 33, no. 4, pp.2102-2111, Dec. 2018.
[14] I. A. A. Afinowi, Z. Q. Zhu, "Hybrid-excited doubly salient synchronous machine with permanent magnets between adjacent salient stator poles," *IEEE Trans. Magn.*, vol. 51, no. 10, pp. 1-9, Oct. 2015.
[15] I. A. A. Afinowi, Z. Q. Zhu, Y. Guan, "A novel brushless AC doubly salient stator slot permanent magnet machine," *IEEE Trans. Energy Convers.*, vol. 31, no. 1, pp. 283-292, March. 2016.
[16] Z. Q. Zhu *et al.*, "Hybrid excited stator slot PM machines with overlapping windings," *2018 XIII International Conference on Electrical Machines (ICEM)*, Alexandroupoli, 2018, pp. 2185-2191.
[17] X. zhao, S. Niu, X Zhang, et al. "Design of a new relieving-DC-saturation hybrid reluctance machine for fault-tolerant in-wheel direct drive," *IEEE Trans. Ind. Electron.*, no. 99, pp.1-1, Nov. 2019.
[18] X. zhao, S. Niu, W Fu, "A new modular relieving-DC-saturation vernier reluctance machine excited by zero-sequence current for electric vehicle," *IEEE Trans. Magn.*, vol. 55, no. 7, pp. 1-5, July. 2019.
[19] Y. Shen, Z. Zeng, Q Lu, "Investigation of a modular linear doubly salient machine with dual-PM in primary yoke and slot openings," *IEEE Trans. Magn.*, vol. 55, no. 6, pp. 1-6, June. 2019.
[20] Y. Shen, "Design and analysis of linear hybrid-excited slot permanent magnet machines," *IEEE Trans. Magn.*, vol. 54, issue. 11, Nov. 2018.
[21] X. Zhao, S. Niu, X. Zhang and W. Fu, "Flux-modulated relieving-DC-saturation hybrid reluctance machine with synthetic slot-PM excitation for electric vehicle in-wheel propulsion," *IEEE Trans. Ind. Electron.*
[22] W. Q. Chu and Z. Q. Zhu, "Average Torque Separation in Permanent Magnet Synchronous Machines Using Frozen Permeability," *IEEE Trans. Magn.*, vol. 49, no. 3, pp. 1202-1210, March 2013.

Jifu Jiang received the B,Sc. degree in electrical engineering from Wuhan University of technology, China, in 2016, and the M.Sc degree from Huazhong University of Science and Technology, China, in 2019. She is currently working toward the Ph.D. degree with the Department of Electrical Engineering, Hong Kong Polytechnic University, Hong Kong. Her research interests include machine design and machine control for electric vehicles and wind power generation.

Shuangxia Niu (Senior Member, IEEE) received the B.Sc. and M.Sc. degrees in electrical engineering from the School of Electrical Engineering and Automation, Tianjin University, Tianjin, China, and the Ph.D. degree in electrical engineering from the Department of Electrical and Electronic Engineering, the university of Hong Kong, Hong Kong. Since 2009, she has been worked with the Hong Kong Polytechnic University, Kowloon, Hong Kong, where she is currently an Associate Professor with the Department of Electrical Engineering. She has authored or co-authored over 100 published journal articles. Her research interests include machine design, renewable energy conversion, and applied electromagnetics.

Xing Zhao (Member, IEEE) received the B.Sc. degree in electrical engineering from Nanjing University of Aeronautics and Astronautics, Nanjing, China, in 2014, and the Ph.D. degree from The Hong Kong Polytechnic University, Hong Kong, China, in 2020. From Jul 2019 to Jan. 2020, he was a Visiting Research Scholar with the Center for Advanced Power Systems, Florida State University, Tallahassee, USA. Between Jul. 2020 and Oct. 2021, he served as a Research Assistant Professor with the Department of Electrical Engineering, The Hong Kong Polytechnic University. Since Nov. 2021, he has been a Lecturer in the Department of Electronic Engineering with University of York, UK. He has authored and coauthored more than 50 articles in the international journals and conferences and holds six granted patents. His research interests include advanced electrical machines, motor drive, and power electronics for electrical vehicles and renewable energy system.